PERGAMON

Journal of Atmospheric and Solar-Terrestrial Physics 63 (2001) 899–914

Journal of ATMOSPHERIC AND SOLAR-TERRESTRIAL PHYSICS

www.elsevier.nl/locate/jastp

Tidal oscillations in the thermosphere: a theoretical investigation of their sources

I.C.F. Müller-Wodarg[a,*], A.D. Aylward[a], T.J. Fuller-Rowell[b]

[a] *Atmospheric Physics Laboratory, University College London 67-73 Riding House Street, London W1P 7PP, UK*
[b] *CIRES, Univ. of Colorado and NOAA Space Environment Laboratory 325 Broadway, Boulder, CO 80303, USA*

Received 8 November 1999; accepted 14 February 2000

Abstract

Measurements of tidal oscillations in the mid to high latitude thermosphere reveal a dependency of diurnal and semidiurnal wind amplitudes on geomagnetic activity. This cannot be explained on the basis of the classical assumption that tides in the lower thermosphere originate primarily from below the mesopause. We use an updated version of the Coupled Thermosphere–Ionosphere–Plasmasphere model (CTIP) to numerically simulate the thermospheric wind oscillations, distinguishing between those propagating upwards through the mesopause and those generated in situ. These simulations suggest that in situ diurnal and semidiurnal oscillations generated at mid to high atitudes by ion-neutral interactions such as ion drag and Joule heating are comparable in magnitude and, towards higher latitudes, stronger than the upwards propagating tides with which they interact through both destructive and constructive interference. Due to their geomagnetic origin, the in-situ oscillations strongly depend on K_p and thus cause an overall K_p dependency in the observed diurnal and semidiurnal winds. We predict the occurrence of measurable in-situ tides also for mid-latitude sites with higher geomagnetic latitude, such as Millstone Hill, during geomagnetically disturbed conditions.

Keywords: Thermosphere; Tides

1. Introduction

Atmospheric tides are global oscillations with periods of one day or a fraction thereof. The most prominent tides found in the terrestrial atmosphere are diurnal (24 h), semidiurnal (12 h) and terdiurnal (8 h). They can be generated either by thermal heating, through processes such as the absorption of solar radiation ("thermal tides") or by the gravitational forcing through the moon and sun ("gravitational tides"). In this study, only thermal tides are considered. Thermal tides are generated where solar heating is important and thus originate from mainly three regions in the Earth's atmosphere, defined by the primary absorbing constituents (Forbes, 1995). Below around 10 km altitude, throughout the troposphere, water molecules absorb in the nearinfrared band. Absorption in the ultraviolet, mainly the Hartley band (200–310 nm) by ozone leads to dissociative heating which peaks between around 40 and 60 km altitude. Molecular oxygen and nitrogen absorb extreme UV radiation in the Schumann–Runge continuum (140–175 nm) at thermospheric heights, leading to peak dissociative heating between 100 and 200 km altitude. In any of these height regimes, the day–night changes in absorption generate Fourier components which are subharmonics of a solar day (24, 12, 8 h, etc.), thus giving a wide range of oscillations, most of which propagate vertically to higher altitudes. Thermal tides also propagate horizontally, typically westward, following the Sun, as opposed to planetary waves which are stationary with respect to Earth. The following study will show that Joule heating can also play an important role in thermally generating oscillations at tidal periods, but we will not refer to these as tides since the Joule heating occurs primarily at mid to high latitudes, while the thermal forcing normally associated with tides is rather a large scale phenomenon. When tides are observed in the lower thermosphere (80–200 km) height regime, they are typically attributed to sources in the middle and lower atmosphere, water and ozone. So, the

* Corresponding author.
E-mail address: ingo@apg.ph.ucl.ac.uk (I.C.F. Müller-Wodarg).

1364-6826/01/$ - see front matter
PII: S1364-6826(00)00202-9

classical understanding is that those tides generated below the mesopause propagate upwards into the thermosphere and ionosphere and significantly influence its energy and dynamics, thus playing an important role in the coupling between the lower- and upper-atmosphere. To conserve momentum and energy, tidal amplitudes increase with height due to the falling density, so once the tides from below the mesopause have reached thermospheric heights they are stronger than those generated in situ in the thermosphere by the oxygen and nitrogen absorption.

An analytical treatment of tidal oscillations in the atmosphere, often referred to as Classical Tidal Theory, was presented by Chapman and Lindzen (1970), Holton (1975) and Volland (1988) and is described further in Section 2.2. Essentially, any latitudinal profile of tidal amplitudes can, according to this linearized theory, be decomposed into Eigenfunctions called Hough modes. Oscillations may be divided into two main categories, the vertically propagating waves and the non-propagating (or evanescent, trapped) ones. Of the tides generated in the lower and middle atmosphere, only the vertically propagating modes will be seen in the thermosphere. These propagating modes have the characteristic that their amplitudes vanish towards the poles, so at high latitudes only weak amplitudes should be found.

Observational evidence presented in Section 3 suggests that some of the diurnal and semidiurnal oscillations found in the lower thermosphere at *E*-region altitudes do not originate from the middle atmosphere, as commonly assumed. The scope of this study is to investigate other potential sources from within the thermosphere, using a numerical model, the Coupled Thermosphere–Ionosphere–Plasmasphere model (CTIP). The model is introduced in Section 2 along with a detailed description of its recently added lower boundary tidal forcing. The observational data from Section 3.1 are compared with the simulations in Section 3.2 and discussed in more detail in Section 4. Section 5 discusses potential limitations of our modelling and concluding remarks are presented in Section 6.

2. The model

2.1. General properties and history

The Coupled Thermosphere–Ionosphere–Plasmasphere model (CTIP) is one of the most comprehensive upper atmosphere models currently available. It solves self-consistently the three-dimensional, time-dependent equations of momentum, energy and continuity for neutral particles (O, O_2, N_2) and ions (O^+, H^+) on an Eulerian co-rotating spherical grid spaced 2° in latitude and 18° in longitude. The neutral gas calculations are carried out on 15 pressure levels between 80 km altitude (1.04 Pa) and, depending on the level of solar and magnetic activity, around 400 km altitude (8.63×10^{-7} Pa), at a resolution of 1 scale height. Ionospheric calculations are carried out in a Lagrangian reference frame along plasma flux tubes on height levels between 100 and 10,000 km, at a resolution ranging from 5 km (at lower altitudes) to 300 km (at the top levels). Parameters relevant to the ion-neutral and neutral-ion coupling are exchanged at every few time steps between the thermospheric and ionospheric codes. These originally separate codes originate from two models developed by different groups in the UK, the thermosphere model by Fuller-Rowell and Rees (1980) and high-latitude ionosphere model by Quegan et al. (1982). They were fully coupled by Fuller-Rowell et al. (1987) to form a version commonly referred to as the Coupled Thermosphere–Ionosphere model (CTIM). This version was later extended to form the Coupled Thermosphere–Ionosphere–Plasmasphere model (CTIP), described by Fuller-Rowell et al. (1996) and Millward et al. (1996). The CTIM differs from the CTIP in that it uses ionospheric parameters from the empirical model by Chiu (1975) equatorward of an adjustable boundary which is normally set to 35° geographic latitude. The CTIP, in contrast, solves the equations of momentum, energy and continuity for ions along closed magnetic flux tubes also at low to mid latitudes, calculating self-consistently plasma densities, temperatures and velocities. A number of important modifications have been added over the years to the CTIM and CTIP and are partly described by Fuller-Rowell et al. (1996) and Millward et al. (1996). A recent extension to the lower boundary of CTIP and CTIM is described in the following. Hereafter, we refer to the CTIP only, but all lower boundary modifications similarly apply to the "non-plasmasphere" version, the CTIM.

2.2. The new lower boundary

As outlined earlier, tides generated in the lower and middle atmosphere propagate into the thermosphere and ionosphere where they form an important source of momentum and energy. Any more comprehensive effort in modelling the upper atmosphere must therefore consider the contribution of these upwards propagating tides. With the CTIP model's lower boundary lying at 80 km, the chemistry involved in the generation of tides from the lower and middle atmosphere cannot be included self-consistently. Thus, it is necessary to account for upwards propagating tides by externally forcing the lower boundary parameters. In principle, any perturbations can be applied as long as the self-consistency in all parameters is ensured, implying that oscillations of pressure must be consistent with those of temperature and winds.

Since global simultaneous measurements of these parameters are not available to-date at sufficient coverage, the use of real data at CTIP's lower boundary is in practise not yet possible. Empirical models, based on measurements, are available but cannot be used either: at present, the most comprehensive ones are the Horizontal Wind Model (HWM) (Hedin et al., 1996) and the MSIS model for temperatures and composition (Hedin, 1991). However, these models are not entirely consistent with each other, so using wind

profiles from one and temperature profiles from the other would not give a self-consistent set of parameters. A third option is to use output from a physical (non-empirical) model as lower boundary conditions. One currently available code which overlaps sufficiently with the CTIP model in terms of altitude and calculates middle atmosphere tides is the global scale wave model (GSWM) by Hagan et al. (1995). In an experimental study, output from this model was successfully used at CTIP Model's lower boundary. The only disadvantage of using two separate codes is of a practical nature: the models run on different computer systems and are operated by different groups, so running a simulation inevitably requires the effort of both parties. When carrying out a large number of simulations, thus, it is more practical to use a self-contained model. More detailed studies involving forcing from the GSWM are planned for the future and are beyond the scope of this study.

A simpler way of implementing external tidal forcing in the CTIP is by using analytical relationships from Classical Tidal Theory, which ensure not only the self-consistency of perturbations in the different parameters but furthermore define their global structure. In spite of some limitations of this approach, as outlined later, it provides a powerful and flexible solution to the lower boundary forcing problem. The core of the mathematical framework used nowadays for describing tidal oscillations in the atmosphere is referred to as Classical Tidal Theory and based on studies by Laplace from 1799 and 1825 which investigated ocean tides. Classical Tidal Theory calculates analytically the atmosphere's response to global perturbations and has been developed considerably since the earliest efforts by Laplace. The theory in its current state is described in detail by Chapman and Lindzen (1970), Holton (1975) and Volland (1988). Essentially, oscillations are applied to parameters in simplified versions of the momentum and energy equations of atmospheric gas particles, giving two differential equations, Laplace's Tidal Equation and the Vertical Structure Equation. The former of these describes the global latitudinal structure of tidal amplitudes, while the latter describes their vertical structure in the atmosphere.

The key assumption made in this theory is that pressure and Coriolis acceleration alone control the motion of gas particles. While this assumption is necessary to ensure that the latitude and height dependencies of oscillations remain mathematically separable and an analytical solution possible, it also forms the principal limitation of the theory. Studies by Chapman and Lindzen (1970) as well as Lindzen and Blake (1972) suggested that Tidal Theory nevertheless reasonably described the behaviour of atmospheric tides up to an altitude of around 100 km. It is known, however, that tides interact non-linearly with the background atmosphere as well as with other families of oscillations, typically gravity waves and planetary waves, so one must be aware of its limitations. However, this does not need to be addressed in the present context: relations from Tidal Theory are used only at the CTIP Model's lower boundary, while at larger heights the tidal propagation is calculated numerically without using any of the theory's assumptions. The Vertical Structure Equation is therefore not used, but only Laplace's Tidal Equation to define the latitudinal profile of amplitudes at the lower boundary height of 80 km.

Laplace's Tidal Equation expresses that any global tidal perturbation profile in an idealized atmosphere can be decomposed into an infinite number of Eigenfunctions, referred to as Hough functions. Following Chapman and Lindzen (1970) and Volland (1988), Hough functions, or Hough modes, are often characterized by a pair of numbers (s,n), where s is the longitudinal and n the latitudinal wave number. Since semidiurnal tides have a longitudinal wave number of 2, the Hough modes describing them are the family of $(2,n)$ modes. Similarly, diurnal tides are described by the $(1,n)$ modes. Even values of n describe modes symmetric to the geographic equator, while antisymmetric modes have odd values of n. Furthermore, the sign of n is important; positive values describe vertically propagating modes, while negative n describes non-propagating, or evanescent modes which are confined to the region of forcing and do not propagate to other altitudes. The value of s, in contrast, is always positive.

Applying linear perturbations to the momentum equation for gas particles controlled by pressure and Coriolis forces alone allows derivation of analytical expressions for the tidal oscillations of winds and temperature. The tidal perturbations of the meridional (u) and zonal (v) wind components, respectively, are given by

$$\Delta u_{s,n}(\theta,t) = \frac{i}{r_E\omega_s(1-(f^2/\omega_s^2))} \times \left[\frac{sf}{\omega_s\cos\theta} - \frac{\partial}{\partial\theta}\right]\Delta\Phi_{s,n}(\theta,t), \quad (1)$$

$$\Delta v_{s,n}(\theta,t) = \frac{-1}{r_E\omega_s(1-(f^2/\omega_s^2))} \times \left[\frac{s}{\cos\theta} - \frac{f}{\omega_s}\frac{\partial}{\partial\theta}\right]\Delta\Phi_{s,n}(\theta,t). \quad (2)$$

Here, the indices s, n are the latitudinal and longitudinal wave numbers (see above), θ is the latitude, t the local time, r_E the Earth's radius and ω_s the frequency of the (s,n) mode. Finally, $f = 2\Omega_E \sin\theta$ is the Coriolis parameter, with Ω_E denoting the Earth's rotational frequency. Since, in accordance with the Tidal Theory requirements, a zero mean wind field must be assumed, Eqs. (1) and (2) represent the absolute values of winds at the CTIP Model's lower boundary, as a function of perturbations in the geopotential, $\Delta\Phi$. The perturbations of geopotential are implemented as global perturbations of the height of the lower boundary pressure layer around an average altitude of 80 km. Following the solution of Laplace's Tidal Equation, the latitudinal structure of these geopotential height oscillations is defined by the Hough functions, and $\Delta\Phi$ is given by

$$\Delta\Phi_{s,n}(\theta,t) = gZ_0^{s,n}\Theta_{s,n}(\theta)e^{i(\omega_s t + s\phi + \phi_0)}, \quad (3)$$

where $\Theta_{s,n}$ are the normalized Hough functions for the (s,n) mode, $Z_0^{s,n}$ are the corresponding geopotential height amplitudes, ϕ_0 their phases (local times of maximum), ϕ is the longitude and g the gravity acceleration. In practise, a global lower boundary perturbation profile is thus defined by merely choosing a set of geopotential height amplitudes and phases for each (s,n) Hough mode. The total wind perturbation field is then given by summing over s and n:

$$\Delta u = \sum_n \sum_s \Delta u_{s,n}, \tag{4}$$

$$\Delta v = \sum_n \sum_s \Delta v_{s,n}. \tag{5}$$

The perturbations of temperature can similarly be expressed as a function of the geopotential height oscillations. Using the hydrostatic equation, the ideal gas law and the vertical structure equation, the expression for global temperature perturbations may be derived to be

$$\Delta T_{s,n}(\theta,t) = \frac{i\alpha}{R}\Delta\Phi_{s,n}(\theta,t), \tag{6}$$

where $R = R^*/M$ is the specific gas constant (R^* being the universal gas constant and M the mean molecular weight of the gas) and α is given by

$$\alpha = \sqrt{\frac{kH}{h_n} - \frac{1}{4}} \tag{7}$$

with $k = 2/7$, H being the scale height and h_n the equivalent depth. The h_n was first introduced in Laplace's study of ocean tides and there referred to the ocean depth. Values for equivalent depth used here are taken from Chapman and Lindzen (1970). As for the velocities, the total global temperature perturbation profile is obtained by summing over s and n:

$$\Delta T = \sum_n \sum_s \Delta T_{s,n}. \tag{8}$$

Since we assume zero mean winds at the lower boundary, the zonal mean temperature must have no latitude dependence either. ΔT in Eq. (8) is thus a global profile of temperature perturbations around a constant lower boundary background value of usually 180 K. Using the above expressions we have implemented temperature perturbations at the model's lower boundary which are physically consistent with the simultaneous wind and geopotential height perturbations.

Note that the square root in Eq. (7) can become negative under certain conditions. The equivalent depth, h_n, of the semidiurnal $(2,2)$ mode has a value of around 7 km, which is larger than that of the diurnal (1,1) and higher-order semidiurnal modes. With typical scale heights of around 6 km near the mesopause one sees that $\alpha^2 < 0$ for the $(2,2)$ mode there, implying that the $(2,2)$ mode at those altitudes is evanescent, or non-propagating. It has been proposed that the $(2,2)$ mode "tunnels"' upwards through this region and is strongly damped until it reaches higher altitudes where it becomes propagating again (P.J.S. Williams, Univ. of Wales, Aberystwyth, private comm., 1997). Temperature perturbations are however calculated at the lower boundary for all other Hough modes.

From expressions (1), (2), (3) and (6) we can derive the phases of temperature and wind oscillations relative to the geopotential height oscillations: temperature and meridional wind phases are shifted by $\frac{1}{4}$ of the tidal period relative to the geopotential phase (i.e. 6 h for diurnal, 3 h for semidiurnal tides), while zonal wind phases are shifted by $\frac{1}{2}$ of the period (i.e. 12 h for diurnal, 6 h for semidiurnal tides). These values are given by the analytical relationships and thus hold only at CTIP Model's lower boundary. At higher altitudes they can be different, depending on how good an approximation linearity is there. One interesting feature in tidal theory is that tidal amplitudes are invariant with longitude. So while parameters such as winds and temperatures do change with longitude, their tidal amplitudes don't, at least under the assumptions of Classical Tidal Theory. Later discussions will show that tidal amplitudes in the lower thermosphere do depend on longitude, so Tidal Theory no longer strictly holds there.

2.3. CTIP simulations

Results presented in the following originate from four simulations with the CTIP Model, two of which use no lower boundary forcing, while the other two use forcing with the $(2,2)$ and $(2,4)$ Hough modes. In the runs with lower boundary tidal forcing the amplitude and phase of the $(2,2)$ mode were set to 200 m geopotential/3.0 h L.T., values for the $(2,4)$ mode were 400 m geopotential/8.0 h L.T.. Relative magnitudes of the $(2,2)$ and $(2,4)$ mode amplitudes and the values for phases are consistent with results from simulations by the Global Scale Wave Model (GSWM) (M. Hagan, private comm., 1999). One pair of tidal and non-tidal simulations is for moderate geomagnetic conditions, with $K_p = 2^+$, while the other pair is for disturbed conditions, using $K_p = 5^-$. Discussions in Section 3.2 will show that the in-situ thermospheric diurnal and semidiurnal oscillations have a strong magnetic activity dependence, and we discuss how the in situ semidiurnal amplitudes compare with those originating from below the mesopause (the "forced" ones). For simplicity we chose not to discuss the relative magnitudes of in-situ and forced diurnal amplitudes and therefore set to zero the diurnal (1,1) mode amplitude at the model's lower boundary. All simulations are for March equinox, with a solar activity level of $F10.7 = 100$. The version of CTIP used in these simulations uses high-latitude auroral ionization and heating from the parameterization by Fuller-Rowell and Evans (1987), which is based on measurements by the TIROS-NOAA satellite, and the high-latitude electric convection field by Foster et al. (1986).

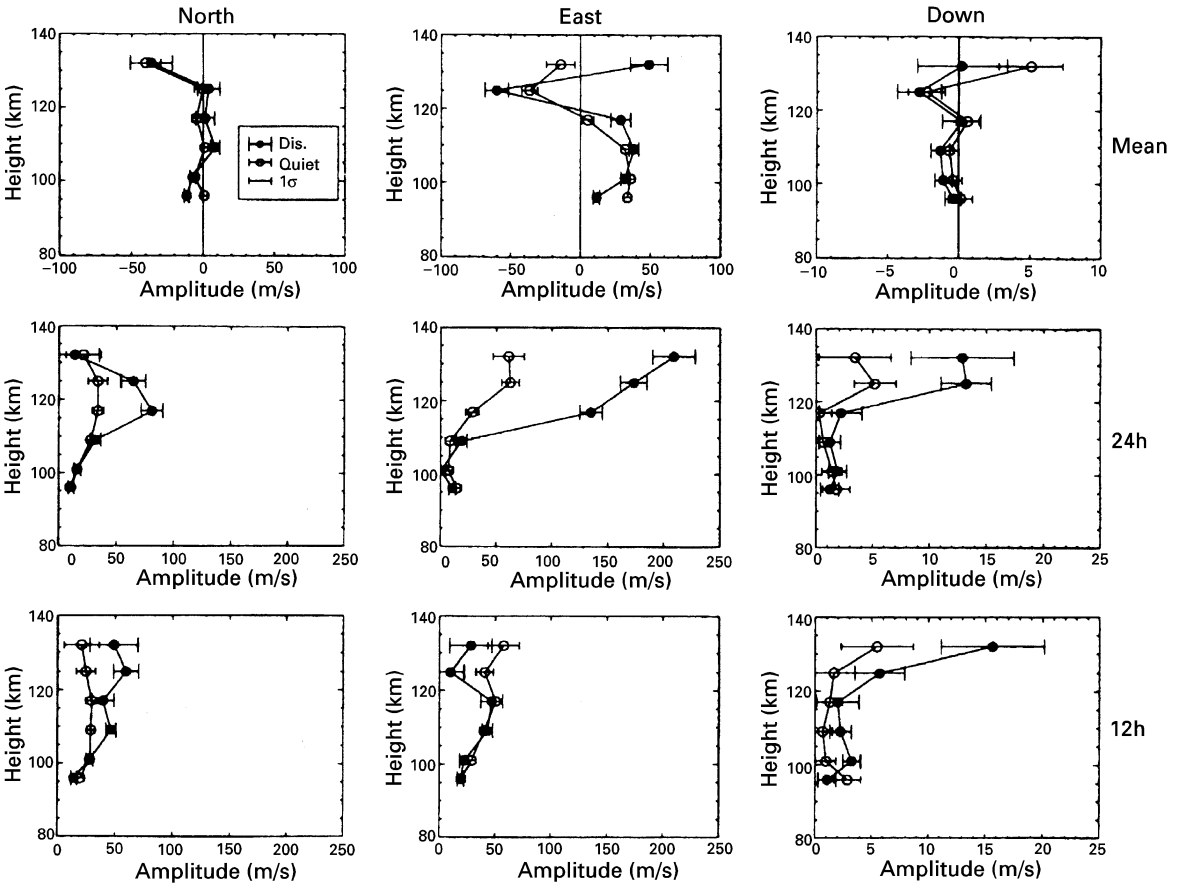

Fig. 1. The variation with height of the northward, eastward and downward neutral wind mean, diurnal and semidiurnal components, as measured by the European Incoherent Scatter Radar (EISCAT) in Tromsø, Norway. Open circles mark geomagnetically quiet and closed circles mark active conditions. (*from* Nozawa and Brekke, 1995)

3. *E*-Region tides and their variability with K_p

3.1. Observational evidence

Fig. 1, taken from (Nozawa and Brekke, 1995), shows height profiles of *E*-region meridional, zonal and vertical wind components measured with the Eiscat facility at Tromsø, Norway (69.6°N, 19.2°E). Panels in the upper row show the mean components, while the second and third rows of panels are the diurnal and semidiurnal components, respectively. Open circles mark values for quiet geomagnetic conditions, while closed circles are values for disturbed conditions. There is no statistically significant variability in the mean meridional and vertical wind components with magnetic activity, while zonal winds change by up to around 20 m/s. Diurnal components, however, vary considerably with magnetic activity, increasing by up to 40 and 140 m/s in the meridional and zonal winds, respectively. Vertical wind amplitudes increase by around 10 m/s. Changes in the semidiurnal components are weaker but nevertheless statistically significant, at up to around 30 and 10 m/s for the horizontal and vertical winds, respectively. Note that diurnal amplitudes generally increase with K_p, while the semidiurnal ones decrease for the zonal winds and increase for the meridional and vertical ones. Horizontal wind amplitudes from the semidiurnal $(2,4)$ Hough mode (see also Section 2.2) peak near 55° latitude, so the amplitudes of the 12 h components in Fig. 1 could represent $(2,4)$ mode oscillations, but their variability with K_p is somewhat puzzling. If indeed the 12 h components in Fig. 1 were $(2,4)$ mode oscillations and thus originated from the lower and middle atmosphere, their variability with K_p would indicate either that regions below the mesopause are considerably influenced by changes in magnetic activity, generating different tidal profiles, or that changes in the background thermosphere with K_p cause a different response to the tidal forcing from below. It is questionable whether geomagnetic activity could have a significant influence on water and ozone absorption in the troposphere and stratosphere, and thus on the tides generated there. This is supported by

output from models such as the HWM (Hedin et al., 1996) which give no variability of the middle atmosphere tidal amplitudes with K_p. Furthermore, results shown in the top row panels of Fig. 1 suggest that dynamical properties of the background atmosphere change very little with K_p. So, the only other plausible option is that the oscillations observed in the lower thermosphere originate not only from the lower and middle atmosphere, but also partly from in-situ sources in the thermosphere which depend on geomagnetic activity.

Kunitake and Schlegel (1991) also investigates the influence of geomagnetic activity on neutral winds derived from Eiscat measurements near 69°N/19°E between 1985 and 1990. They found a correlation between changes in K_p and the diurnal wind amplitudes for heights around 120 km, but not below. Also, they found the semidiurnal amplitudes to increase with K_p for the meridional wind component, but not for the zonal winds, in agreement with findings by Nozawa and Brekke (1995). The influence of K_p on the tidal amplitudes at high latitudes was also investigated for summer conditions at Chatanika (65°N/147°W) by Johnson et al. (1987). In their analysis, diurnal amplitudes generally increased with K_p between 109 and 115 km, while the semidiurnal ones decreased.

Fesen (1997) carried out a comprehensive modelling study to investigated the effects of K_p on thermospheric tides for different seasons at solar cycle minimum and maximum, using the National Center for Atmospheric Research Thermosphere–Ionosphere General Circulation Model (NCAR-TIGCM) and confirmed the general trend found in the observational studies. The modelling study found the strongest influence of K_p to occur at mid to high latitudes. However, the author made no investigation regarding possible sources of these oscillations.

3.2. Results from CTIP simulations

In the following CTIP simulations, no attempt is made to reproduce exactly the data of Fig. 1, but the emphasis lies rather on finding similar trends, particularly in the variability with K_p, and understanding the underlying processes. All amplitudes and phases presented in the following were extracted from the CTIP simulations by the classical method of Fourier decomposition. Fig. 2 shows the meridional, zonal and vertical components of neutral wind on the model grid point closest to Tromsø, at 70°N/18°E, during geomagnetically moderate ($K_p = 2^+$) and more active ($K_p = 5^-$) conditions (upper and lower panels, respectively). The simulations in Fig. 2 were carried out without lower boundary tidal forcing. All values are shown for pressure level 6, corresponding to 7×10^{-3} Pa pressure or between 115 and 120 km altitude, thus representing roughly *E*-region conditions. The solid lines in Fig. 2 represent the vertical velocities (positive upward), which for easier display have been multiplied by a factor of 100. Dashed lines are the zonal components (positive eastward) and dotted lines are the meridional ones (positive southward).

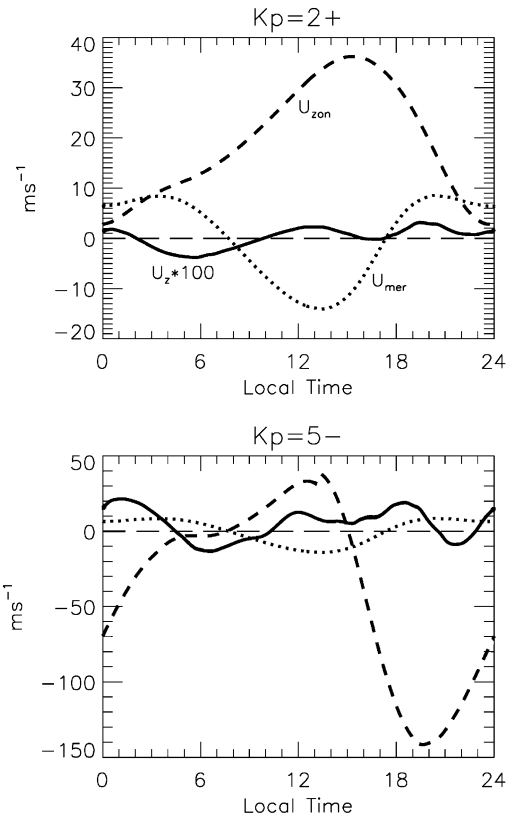

Fig. 2. Neutral winds at 70°N/18°E and 115–120 km altitude, as simulated by the CTIP model for geomagnetically moderate (upper plot) and active (lower plot) conditions. Dashed lines are zonal (positive eastward) and dotted curves are meridional (positive southward) winds. The solid lines are vertical winds multiplied by 100. The plot shows March equinox conditions.

For $K_p = 2^+$ the meridional winds (dotted line) have a considerable semidiurnal component superimposed on the diurnal behaviour, blowing northward between around 6 and 18 h L.T. and southward throughout the night, maximizing near 20 h and 4 h L.T. Note that the values in Fig. 2 derive from a run without tidal forcing, so the semidiurnal behaviour in meridional winds is generated in-situ in the thermosphere. Zonal winds are primarily diurnal, blowing towards the east throughout the day, peaking in the afternoon sector near 17 h L.T. Vertical winds appear to have a noticeable terdiurnal component, with peak upward velocities at around 1, 13 and 20 h L.T., reaching values of less than 0.05 m/s.

For $K_p = 5^-$ (lower panel in Fig. 2) the general behaviour of vertical winds is similar, but now values are larger at up to 0.3 m/s. Meridional winds direction changes very little with K_p. Considerable differences are seen in the zonal winds which for higher K_p blow eastward only between around 8 and 15 h L.T., thereafter being strongly westward, reaching peak values of 140 m/s near 20 h L.T. Furthermore, the

overall behaviour of zonal winds is clearly more semidiurnal at the higher K_p.

Fig. 3 shows diurnal and semidiurnal amplitudes of the horizontal wind components between 80 and 320 km altitude, as simulated by the CTIP model at 70°N/18°E. Solid curves are for geomagnetically moderate, the dashed ones are for more active conditions. Output is again taken from the runs without lower boundary forcing and thus represent tidal amplitudes generated in situ only above 80 km. In the following we compare the simulated amplitudes with those of Fig. 1. Quiet-time semidiurnal amplitudes in Fig. 1 lie around 20 and 50 m/s for the meridional and zonal winds, respectively, while the corresponding values from Fig. 3 for the same height range (80–135 km) are 10 and 20 m/s. For active conditions zonal and meridional amplitudes at those heights are around 50 m/s for the data and between 20 and 60 m/s for simulations. Both in terms of values and vertical profiles the agreement between measurements and model is better during active conditions, while the quiet-time values are considerably smaller in the model. Diurnal amplitudes generally correspond better than the semidiurnal ones, in spite of the absence of diurnal lower boundary forcing, suggesting that large part of diurnal oscillations in the lower thermosphere may be generated in-situ. When comparing Figs. 2 and 3 note that the pressure level of Fig. 2 is at an altitude of around 115 km for $K_p=2^+$ and 119 km for $K_p=5^-$. To illustrate this more clearly, the pressure level has been marked with a square in Fig. 3. Considering this, the spectral analysis in Fig. 3 confirms the trends with K_p described earlier for Fig. 2, illustrating the strong increase of 12 h amplitudes, particularly in the zonal winds, and similar increase in the 24 h components. At pressure level 6 (marked in Fig. 3) the 12 and 24 h components are similar in magnitude, which is why the semidiurnal behaviour is clearly seen in Fig. 2 and not simply a hidden higher harmonic.

The remarkable point of results in Figs. 2 and 3 is that tidal oscillations are present at those heights in the thermosphere in spite of the absence of forcing from below the mesopause, and that they show a strong dependency on K_p. This suggests that in-situ tidal sources appear to play an important role in the thermosphere, particularly during geomagnetically active conditions. While harmonic analyses *per se* are often rather academic, with many of the higher harmonics often not appearing as "real behaviour" in the "raw" values, Fig. 2 shows that one can observe "true" semidiurnal behaviour in some of the wind components as a result of in-situ thermospheric processes alone. In the real atmosphere the simulated situation of "no forcing from below" does not exist, but the advantage of using a numerical model such as the CTIP is to be able to separate processes and "isolate" the thermosphere, which helps us to understand better the underlying physics.

Fig. 4 shows the same amplitudes as Fig. 3, but from two simulations which include semidiurnal lower boundary forcing. The response in the diurnal amplitudes is very similar below 140 km altitude in the "forced" (Fig. 4) and "unforced" (Fig. 3) simulations, which is plausible since the forcing is with semidiurnal oscillations only and not diurnal ones. However, differences are present above those heights, suggesting non-linear interactions between the diurnal and (changed) semidiurnal oscillations or the diurnal oscillations with the (also changed) background atmosphere. The semidiurnal amplitudes below 120 km in Fig. 4 are larger than those in Fig. 3, as expected, and compare better to the observations of Fig. 1. Interesting comparisons between Figs. 3 and 4 are the differences in responses of meridional and zonal winds to changes in K_p. While in the unforced case (Fig. 3) the semidiurnal amplitudes generally increase with K_p, we find an occasional decrease in the meridional wind components in Fig. 4 and, depending on altitude, a weaker increase than in Fig. 3. The semidiurnal zonal wind amplitudes also respond differently, not increasing as much with K_p as in the unforced case. The opposite trends in the responses of the different wind components are in agreement with the data of Fig. 1, even though there it is the zonal component decreasing with K_p, not the meridional one as in the simulations. A interesting result from these simulations is that combining lower boundary forcing with the in-situ oscillations leads to a more realistic behaviour, implying that both sources are important.

When comparing diurnal amplitudes of Figs. 3 and 4 to the measured ones in Fig. 1 we see that there is some discrepancy above 120 km at high levels of magnetic activity. While measured diurnal amplitudes of measured zonal winds increase with altitude to values of around 200 m/s at 140 km, the simulated only reach around half those values. Instead, the meridional wind amplitudes reach around 200 m/s in the simulations, as opposed to 70 m/s in the data. One possible explanation for this might be the difference between the simulated and real high-latitude convection pattern and locations of the auroral oval. The exact direction of ion drifts will during geomagnetically active conditions have an important influence on the neutral wind direction as well. However, since our aim here is to merely show the trends in amplitudes with changing K_p a more detailed analysis of these discrepancies is beyond the scope of this study.

In order to gain a more global view of thermospheric semidiurnal oscillations, Fig. 5 shows 12 h amplitudes and phases of zonal winds without tidal forcing from below (first row of panels) and with lower boundary tides (second row), for geomagnetically moderate conditions ($K_p = 2^+$). The plots are latitude–height profiles at the fixed longitude of 18°E. The upper left panel reveals that in situ semidiurnal oscillations are strongest at mid to high latitudes, poleward of around 50° geographic latitude, or 47° geomagnetic latitude. Peak amplitude values are around 110 m/s above 200 km, but values range around 10–80 m/s between 120 and 200 km. Below 120 km there is virtually no in situ forcing. Equatorward of 50°, weak semidiurnal in situ oscillations are found only above 140 km altitude. The corresponding phase plot (upper right panel) shows constant phases with height above around 160 km altitude, suggesting that the

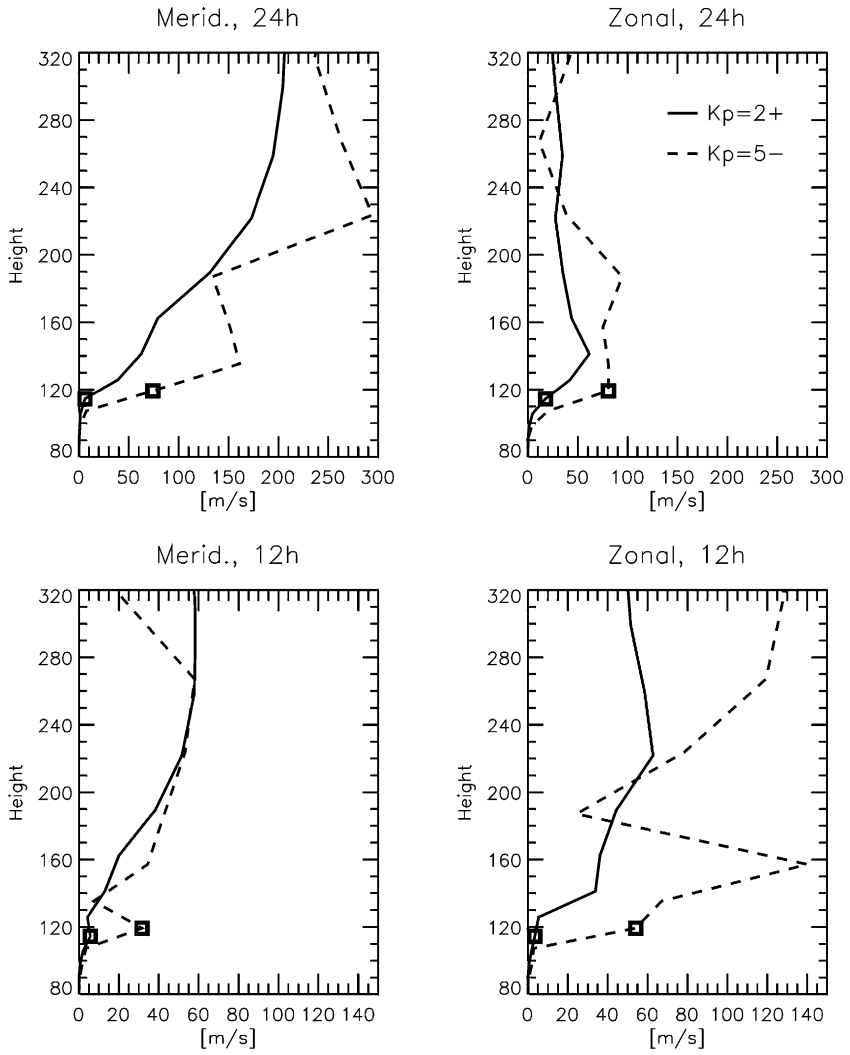

Fig. 3. Diurnal and semidiurnal in-situ horizontal wind amplitudes for geomagnetically moderate (solid) and active (dashed) conditions, as simulated with the CTIP. Boxes indicate pressure level 6, as used in Figs. 2, 7 and 8.

semidiurnal in situ oscillations there are non-propagating. Above 160 km the phases poleward of around 60° do however change with latitude at a rate of roughly 3 h per 10° latitude. When comparing the semidiurnal phases at the same height but different latitudes, thus, the lower latitude site has a different (earlier) phase according to the simulations. Below around 160 km, in-situ semidiurnal phases also change with height, so the oscillations are vertically propagating. One can derive the vertical phase velocity to have values between 0.5 and 3 m/s, depending on latitude, and the oscillations have a vertical wavelength in the order of 60–100 km. Phase values below 120 km in the upper right panel have no relevance since amplitudes there are very small.

The lower row of panels in Fig. 5 shows the same profiles of amplitudes and phases, but from the simulation which included lower boundary tidal forcing. Semidiurnal oscillations are now also found below 120 km, particularly at low to mid latitudes. Comparison of the upper and lower amplitude panels shows how in situ and external tides compare at different latitudes and heights. One sees that the lower boundary tides propagate up to altitudes of around 160 km in the zonal winds, with peak amplitudes near 130 km. This behaviour is also confirmed by the phase plot (bottom right panel). As tides propagate through the mesopause into the lower thermosphere, their amplitudes increase to a critical value, until non-linear processes lead to their dissipation and release of their momentum and energy to the background atmosphere. As a result, tidal amplitudes reach a peak and then decrease with height, as seen in Fig. 5. This behaviour is well known and has been observed in numerous tidal

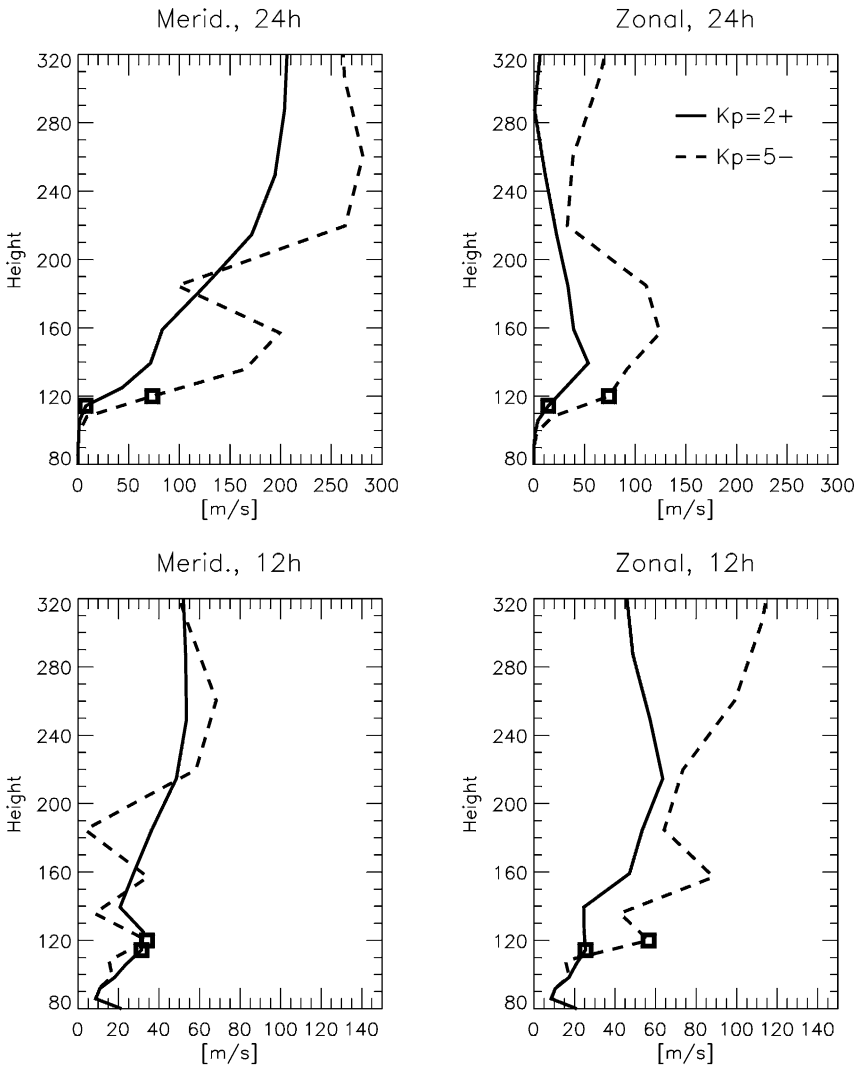

Fig. 4. Same as Fig. 3, but for simulations which include lower boundary semidiurnal tidal forcing.

studies, such as those by Nozawa and Brekke (1995) or Goncharenko and Salah (1998). The phase plot shows that tides from below are westward propagating up to around 120 km at low- and 130 km at mid-latitudes, reversing direction above that, becoming eastward propagating until they disappear almost entirely.

Another interesting feature of Fig. 5 is the latitudinal asymmetry in the amplitude profiles: northern hemisphere patterns are generally shifted towards lower latitudes by around 10°, compared with the southern hemisphere patterns. This may be attributed to the offset of the geomagnetic and geographic poles which causes the northern auroral oval to reach down to lower geographic latitudes than the southern aurora at this particular longitude of 18°E. In the "Asian" longitude sector (around 90° − 130°E) the southern magnetic pole reaches to lower geographic latitudes than the northern one, so there the corresponding amplitude patterns are reversed, shifted towards the north. This again strongly supports the idea that the ion-neutral interactions at high latitudes play a key role in the generation of these oscillations.

In the following, we investigate further the longitudinal structure of oscillations. Fig. 6 shows diurnal and semidiurnal amplitudes of zonal winds at the geographic latitude 42°N versus longitude and height. We chose this particular latitude since it corresponds to that of the Millstone Hill observatory (42.6°N/71.5°W), from which extensive tidal Incoherent Scatter Radar measurements are carried out in the *E*-region. Values are from the simulation with $K_p = 5^-$ and lower boundary forcing enabled. We now look at this to learn more about the oscillations at mid-latitudes, but most of the following discussion which refers to longitudinal

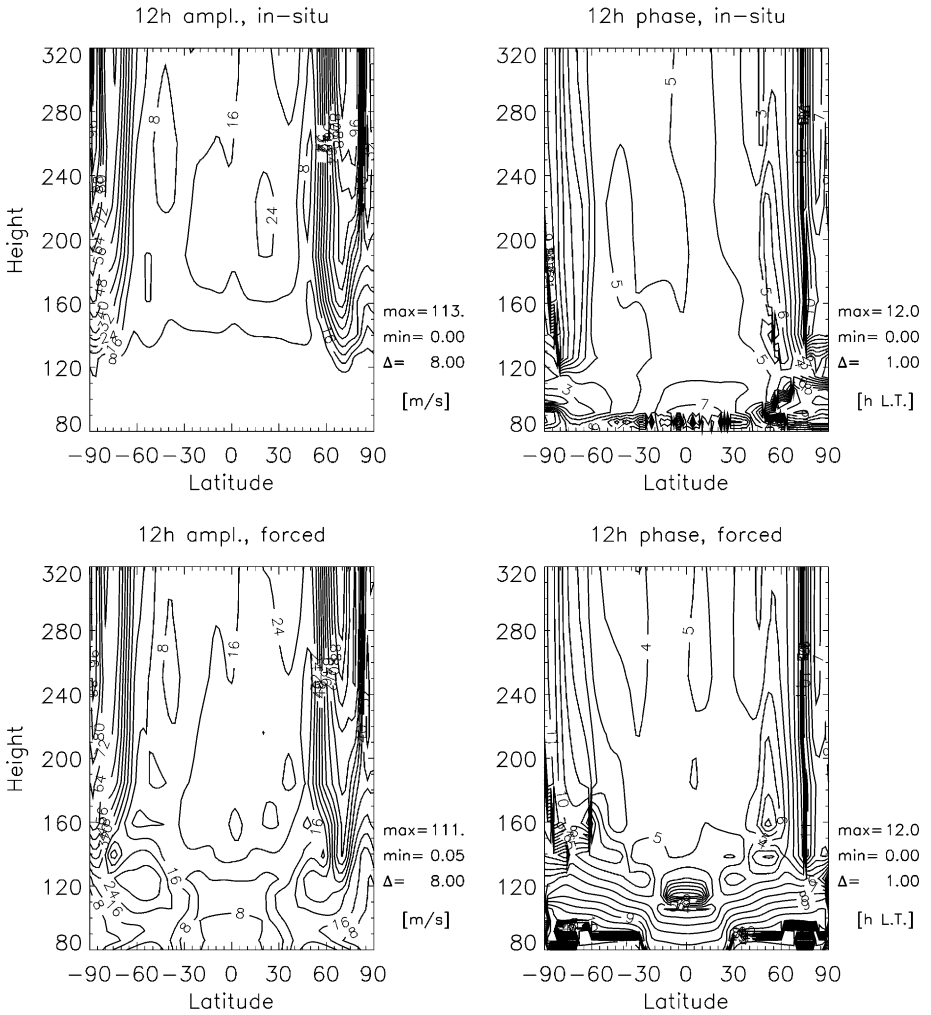

Fig. 5. Zonal wind semidiurnal amplitudes and phases, as simulated by the CTIP without (upper row of panels) and with (lower row) tidal forcing from the mesopause. Values are shown for the 18°E longitude sector during geomagnetically moderate conditions in March. Phase values below 120 km in the upper right panel can be ignored since amplitudes there are negligible.

structures similarly applies at the higher latitude of 70°N which we investigated previously. The simulation used for Fig. 6 includes the lower boundary tidal forcing. Since only the simulation with tidal forcing is shown, we use the longitudinal structure of tidal amplitudes as an indicator for distinguishing between the oscillations originating from the lower boundary forcing and those generated in situ. As mentioned in Section 2.2, Classical Tidal Theory claims that tidal amplitudes are invariant with longitude, so the lower boundary forcing inevitably has the same property. Forced tidal amplitudes are thus longitude-invariant while simulations presented earlier suggested that the in situ ones changed with longitude.

The phase plots in Fig. 6 suggest that oscillations at that latitude are vertically propagating below around 200 km altitude, while above that the contour lines are primarily vertical and the phases thus constant with height. The important features in the amplitude panels are the longitudinal and height structures of the patterns. Both the diurnal and semidiurnal amplitudes are strongest in the "American sector", centred around 60°W, which is roughly the longitude of the northern geomagnetic pole, supporting again the idea of geomagnetic sources for the oscillations. A key argument in favour of an "in-situ" origin of these amplitude peaks in the American sector is that the features do not occur in simulations with identical forcing from below, but lower K_p (not shown). Furthermore, the diurnal amplitude peak (upper left panel in Fig. 6) coincides in longitude and altitude with the semidiurnal one (lower left panel in Fig. 6), suggesting a common origin. Since we use no diurnal lower boundary forcing in these runs, the diurnal amplitude feature in Fig. 6 cannot be generated by upwards propagating

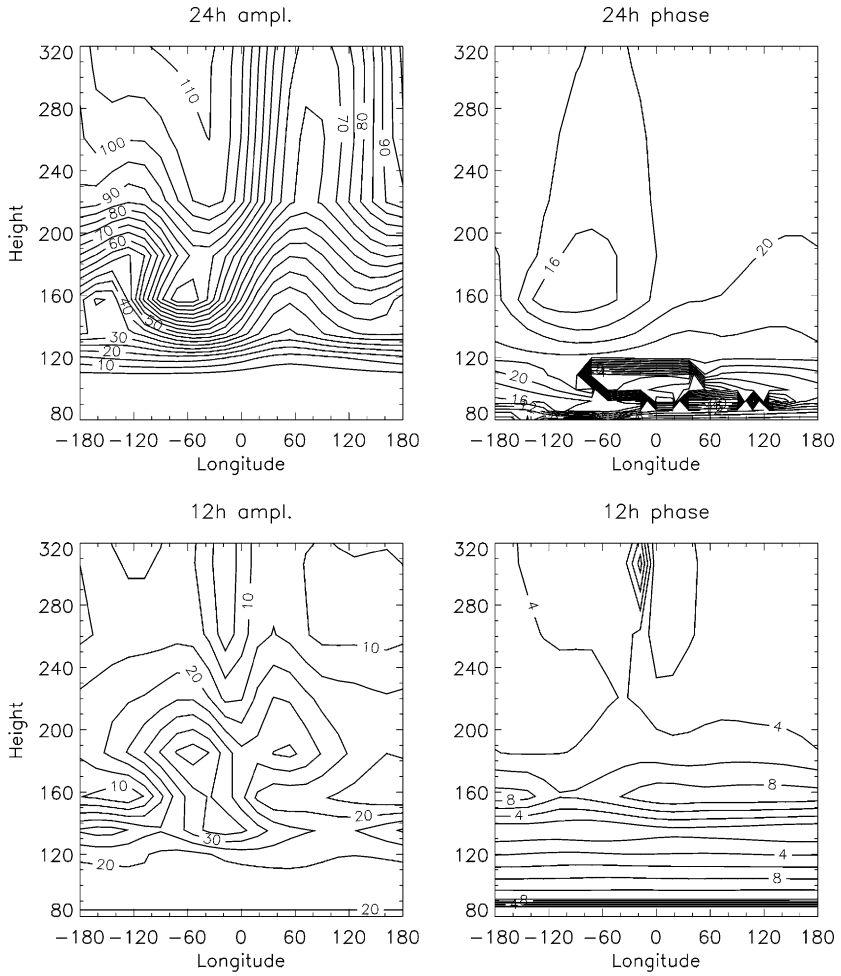

Fig. 6. Zonal wind diurnal and semidiurnal amplitudes at 42°N, as simulated by the CTIP during geomagnetically active conditions. Lower boundary semidiurnal tidal forcing is included. Diurnal phases below 110 km altitude (top right panel) can be ignored as amplitudes are negligible.

tides. Below 120 km altitude in Fig. 6 there is hardly any longitude dependency of the semidiurnal amplitudes (contour lines in the plot are horizontal), so those amplitudes derive from the lower boundary forcing.

A key finding from Fig. 6 is that in-situ oscillations, which cause the amplitude peaks in the American sector, are important also at the lower latitude of 42°N for a sufficiently high level of geomagnetic activity, while we previously discussed such behaviour for the higher latitude of 70°N only (Figs. 2–4). In terms of geomagnetic latitudes the American sector shown in Fig. 6 lies at around 53°N, while Figs. 2 and 3 are near 67°N. So, in terms of geomagnetic latitude the distance between the sites is less than in terms of geographic latitude, which matters if the in situ oscillations are indeed geomagnetically controlled. For lower levels of K_p we found only weak in situ semidiurnal oscillations at 42°N (not shown), suggesting that most of the 12 h oscillations observed there originate from the middle atmosphere. So, as long as K_p values will not exceed a threshold value, no variation of semidiurnal oscillations with K_p should be observable. The physical significance of such a threshold value lies in the spatial distribution of the ion convection pattern and strength of the electric convection field. The K_p dependence of semidiurnal oscillations is clearly caused by the ion-neutral interactions through collisions, and as long as the "overhead" electric fields are too weak the ions will simply follow the neutral solar-driven gas motion. It will be a useful exercise to comprehensively analyse the K_p dependency of measured 12 h oscillations for different latitudes. A preliminary investigation of tidal measurements with the Millstone Hill incoherent scatter radar revealed no clear trend in tidal variability with K_p (J. Salah, Haystack Observatory, M.I.T., Private Comm., 1999).

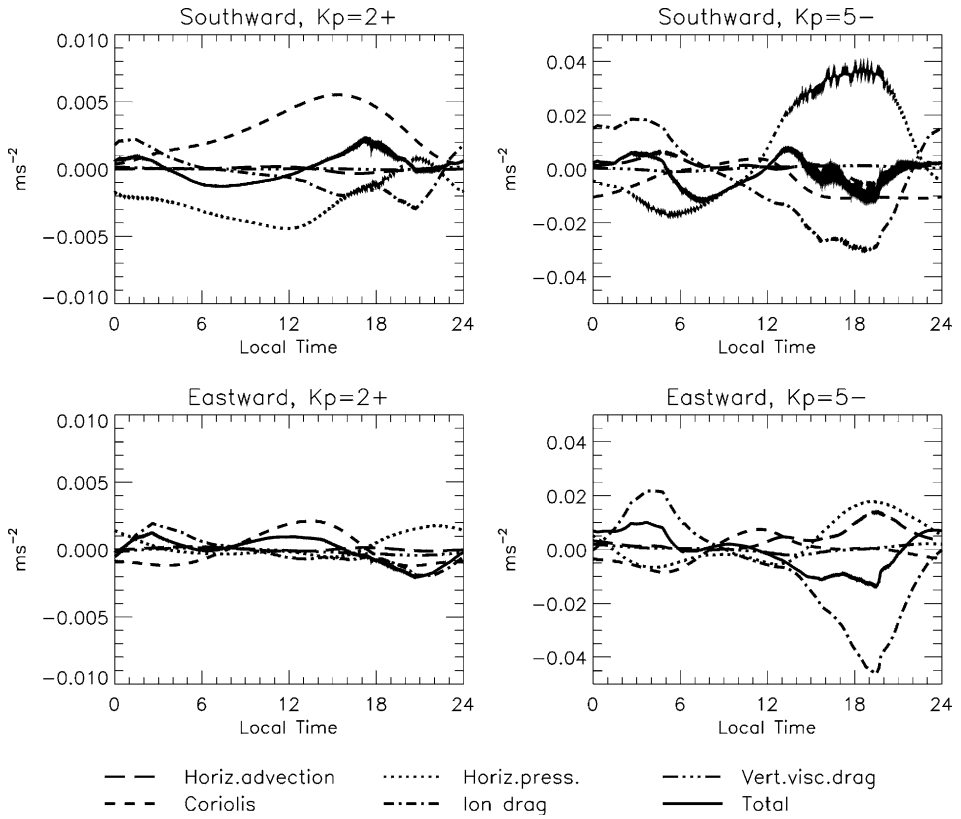

Fig. 7. Meridional (positive southward) and zonal (positive eastward) acceleration terms at 70°N/18°E on pressure level 6 (115–120 km), as simulated by the CTIP for geomagnetically moderate (left column) and active (right column) conditions. The simulation uses no lower boundary tidal forcing, so all terms represent in situ forcing only.

4. Drivers of diurnal and semidiurnal oscillations within the thermosphere

4.1. Acceleration terms

In order to analyse in more detail the processes underlying the results described in the previous section, Fig. 7 displays the key acceleration terms versus local time at 70°N/18°E for moderate (left column) and disturbed (right column) geomagnetic conditions. Terms in Fig. 7 are taken from simulations without lower boundary tidal forcing. Values are shown for the same pressure level as Fig. 2, so they represent roughly *E*-region conditions. The momentum equation used in the CTIP model is described in detail by Fuller-Rowell and Rees (1980) as well as Fuller-Rowell et al. (1996).

For moderate K_p of 2^+ (left column), the meridional components of pressure gradient (dotted line) and Coriolis force (narrow–dashed line) roughly balance throughout most of the day. The zonal components are somewhat more complex, with Coriolis force being balanced both by pressure gradients and ion drag (dashed–dotted line). In the meridional component ion drag plays a role from early afternoon to early morning hours only. Overall, ion drag is primarily northward during the afternoon hours and towards north-west during early evening, switching to south-east round about midnight until early morning. Note that the detailed behaviour of the ion drag term is, as mentioned earlier, very sensitive to the exact shape of the convection pattern. Similarly, the term is dependent on the location of the auroral oval since large ion velocities within the oval lead to strong ion-neutral coupling and thus significant ion drag. The acceleration terms in Fig. 7 are primarily diurnal in their behaviour, but higher harmonic components are present in the ion drag and pressure terms. Looking at their sum (solid line), though, a clear semidiurnal behaviour is found. So, it is rather the combination of terms than any one on its own which generates an overall semidiurnal behaviour in the accelerations.

For disturbed conditions (right column in Fig. 7) the balance of forces is quite different. Here, ion drag is much stronger, both in absolute and relative terms, and often balances the pressure gradient with Coriolis acceleration relative to the others being considerably smaller than during geomagnetically moderate conditions. The *E*-region momentum balance was also studied theoretically by Larsen and

Walterscheid (1995) and experimentally by Maeda et al. (1999), who similarly found the potential importance of the ion-neutral coupling term, in agreement with our findings. With ion drag roughly balancing pressure gradients, the overall flow is during active conditions almost perpendicular to the isobars. Adding all the acceleration terms (solid line) again gives a primarily semidiurnal behaviour, even though individual forcing terms are mainly diurnal. One exception to this is the zonal pressure gradient which is more semidiurnal than was found for geomagnetically moderate conditions. A further interesting difference between the active and moderate conditions lies in the direction of the meridional pressure gradient: while for the moderate case (upper left panel of Fig. 7) it is northward throughout most of the day, except for a slight southward "kick" centred around 21 h local time, for active conditions it is northward only after midnight until around noon and then switches to southward until midnight. Horizontal pressure gradients are controlled by horizontal temperature gradients, so in the following we will thus discuss in more detail the heating terms.

4.2. Heating terms

In the following we will describe the behaviour of various heating terms in our simulations. A detailed description of the energy balance equation used in CTIP Model was given by Fuller-Rowell and Rees (1980) and Fuller-Rowell et al. (1996). Fig. 8 shows heating rates for the same pressure level and location as Fig. 7 during geomagnetically moderate (upper panel) and active (lower panel) conditions. For $K_p = 2^+$ (upper panel) one striking feature is the importance of adiabatic heating and cooling (dotted lines) with a clearly semidiurnal behaviour, peaking near 6 h and 16 h L.T. Physically, adiabatic heating and cooling are a result of air parcels being displaced vertically relative to pressure levels and result from the compression or expansion of the parcel, respectively. The heating results from downwelling, whilst cooling results from upwelling relative to pressure levels. The up and downwelling, in turn, are a result of converging and diverging horizontal winds (see also Rishbeth and Müller-Wodarg, 1999), leading to their name of "vertical divergence winds", so changes in the horizontal wind field appear to have an important effect on the energetics, too, which then in turn again affect the dynamics. This example illustrates nicely the close coupling between dynamics and energetics in the *E*-region.

General Circulation Models such as the CTIP are known to generally underestimate vertical winds compared to measurements, mainly because of the lack of fine structure and thus short-scale changes. In Fig. 2 the vertical winds under moderate geomagnetic conditions were found to be tiny, in the order of a few centimetres per second, while those of Fig. 1 are in the order of several metres per second. Still, they cause the relatively strong adiabatic heating and cooling in the simulations, which is also confirmed when comparing the vertical wind curves in Fig. 2 with the adiabatic

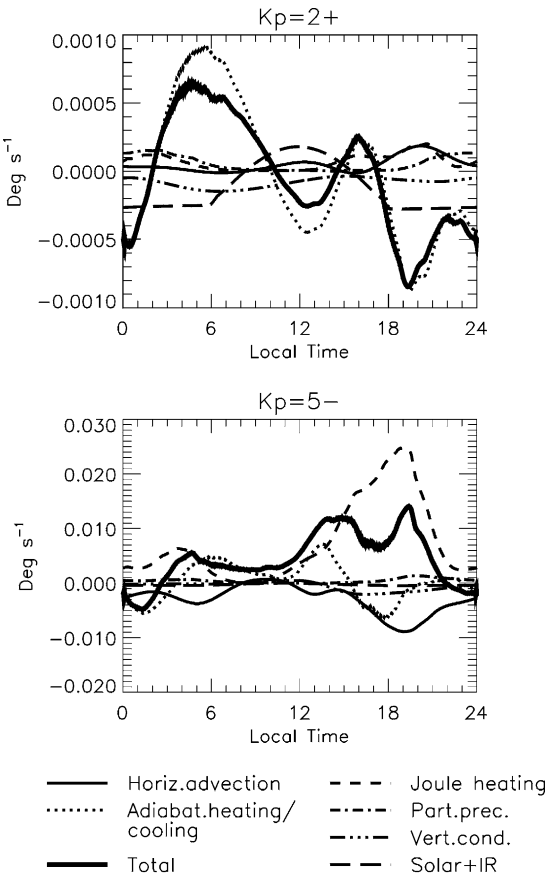

Fig. 8. Same as Fig. 7, but heating terms.

heating terms in Fig. 8. The comparison shows that downward winds cause heating and upward winds adiabatic cooling in the model, as expected from theory. So, it may be that in the real world, where vertical winds are stronger, the importance of adiabatic processes in the *E*-region is even larger than we found here. Note that vertical winds in Fig. 2 are the sum of the divergence wind, which causes the adiabatic heating, but also include the "barometric" component, which is due to the expansion and contraction of the atmosphere, or the change of altitude of a pressure level with time (Rishbeth and Müller-Wodarg, 1999). The barometric wind component does not cause any adiabatic heating, but we found it to be considerably smaller than the divergence wind in our simulations, so the vertical winds of Fig. 2 are to a good approximation equal to the divergence wind only. In the CTIP model, adiabatic heating is calculated using the divergence winds only.

Joule heating (narrow–dashed lines) along with particle precipitation (dashed–dotted lines) contribute only from late afternoon to early morning, but as described earlier in the case of ion drag the exact magnitudes and time behaviour very much depend on the convection field pattern and location relative to the auroral oval. The lower panel of Fig. 8

illustrates the strong dependency of Joule heating on magnetic activity: for more disturbed conditions ($K_p = 5^-$) it is the dominant source of heat during the afternoon and night at this latitude. This Joule heating strongly controls the southward pressure gradient during active conditions, as shown in the top left panel of Fig. 7, becoming more important in our simulation than the solar heating contribution.

So, horizontal winds (see Fig. 2) are primarily solar-controlled for quiet and moderate conditions, flowing from the day to nightside during late afternoon/early evening hours, but for high K_p the strong westward ion drifts may cause a reversal of the neutral zonal velocities from the night to dayside, as seen in Fig. 2, and considerable Joule heating also affects the dynamics. Vertical conduction of heat is small but not insignificant, especially during nighttime. The effects of evening zonal winds on the energetics is illustrated through the horizontal energy advection term (narrow solid lines) in Fig. 8: for $K_p = 2^+$ heat is transported from the hotter dayside towards the evening sector, providing an important source of energy there, while for high K_p (lower panel in Fig. 8) winds blow from the cooler nightside towards the dayside, thus cooling the evening sector. The strong solid line in Fig. 8 represents the sum of all terms, and thus the total heating rate. Even without any tidal forcing from the middle atmosphere the total heating is clearly semidiurnal, caused by a combination of Joule heating, adiabatic heating and horizontal energy transport.

5. Potential limitations of our simulations

The CTIP is a physical, self-consistent model which reproduces well the key processes taking place in the thermosphere. However, fully coupled models such as the CTIP in general often lack detail, due to limitations in computer processing power, so many processes occurring in the real thermosphere are ignored here, in particular those which require finer spatial resolution than the 2° by 18° grid used in the CTIP code. In the simulations presented here we also have not included other families of oscillations such as gravity and planetary waves except for those generated in-situ. These waves are known to play an important role in the thermosphere, influencing also the tides through non-linear interactions (Teitelbaum and Vial, 1991). Such interactions, in turn, might affect the phases of tides, which would affect the interaction of in-situ and middle atmosphere tides. Also, the dynamical ion-neutral coupling at low latitudes is not fully addressed in the model: the calculations here were made using parameterized low-latitude electric fields by Richmond et al. (1980), and we thus ignored the dynamo effect which may play an important role in transferring tidal oscillations from the neutral atmosphere into the ionosphere through modulations of the electric field. It is unlikely, though, that this coupling will noticeably affect the neutral atmosphere tides addressed in this study.

Cooling through 5.3 μm emissions by NO in the lower thermosphere is known to play an important role during geomagnetically active conditions (Field et al., 1998; Wells et al., 1997; Maeda et al., 1989), but is not included as a separate cooling term in our current simulations. To account roughly for the effects of NO cooling, the heating efficiency used in the CTIP model is adjusted in that it is reduced considerably below 200 km altitude (see Fig. 2 in Wells et al., 1997). Effects of a more accurate treatment of NO cooling on simulated high-latitude thermospheric winds, temperature and composition were presented by Wells et al. (1997). In essence, inclusion of more accurate NO cooling reduced the diurnal wind amplitudes by around 25% at *F*-region altitudes. Exospheric temperatures were also reduced by around 25% and mean molecular mass by 10%. We believe that a more accurate treatment of NO cooling might also affect the magnitudes of semidiurnal and diurnal in situ amplitudes presented here, but not the overall effect of magnetic activity on tidal amplitudes which is the key issue discussed in this study.

6. Concluding comments

Prompted by observations which suggest that diurnal and semidiurnal oscillations in thermospheric winds at mid to high latitudes are affected by the level of geomagnetic activity, we have used the CTIP Model to investigate the processes causing this behaviour. While the classical idea is that most of the diurnal and semidiurnal oscillations observed in the lower thermosphere originate from the stratosphere and mesosphere, we have shown that for mid to high latitudes above 120 km in situ generated oscillations cannot be ignored. They are generated by the additional Joule heating and ion drag acting upon the background atmosphere. While neither of these two on their own appear explicitly semidiurnal, it is their interaction with the solar-controlled background atmosphere which overall gives a significant semidiurnal component. Also, we found a strong semidiurnal component in the adiabatic heating term at *E*-region heights, caused by divergence in the horizontal wind field which generates vertical winds. Since both Joule heating and ion drag are strong in the auroral regions, the in situ forcing has not only a distinct latitude dependency but also a longitudinal variation due to the offset of the geographic and geomagnetic poles. As a result, we find substantial in-situ oscillations in the "American" longitude sector down to mid-latitudes for active geomagnetic conditions, while the same is not the case for the same geographic latitude in the "Asian" longitude sector. So, in-situ-generated oscillations are oriented geomagnetically rather than geographically.

Our simulations showed that upwards propagating tides interact with those generated in-situ, causing either constructive or destructive interference, depending on the relative phases. So, while in-situ diurnal and semidiurnal oscillations on their own would generally increase with K_p, the addition

of upwards propagating tides revealed a more complex picture with both lower and higher amplitudes at different locations during higher K_p, in agreement with observations by Nozawa and Brekke (1995), Kunitake and Schlegel (1991) and Johnson et al. (1987). The presented study showed one particular situation and the response in reality very much depends on the exact shape of the high-latitude electric convection field, the location of the aurora as well as the exact amplitudes and phases of tides propagating upwards through the mesopause. While the general trend is to expand the numerical models to cover a larger height range, the aspect of the CTIP Model's lower boundary being at 80 km allowed us to isolate the thermosphere and thus clearly distinguish between oscillations generated in-situ and those propagating upwards through the mesopause, which are included as optional lower boundary forcing in the model.

We found the in-situ generated diurnal and semidiurnal oscillations to be vertically propagating below around 200 km altitude and non-propagating above that. Given furthermore that they are generated and occur primarily at high latitudes we have generally in this study not referred to them as tides, which in the classical definition are global propagating and non-propagating oscillations generated thermally or gravitationally. Nevertheless, these oscillations were found to interact with the upwards propagating tides, thus affecting their global profiles.

Acknowledgements

I.C.F. Müller-Wodarg has been funded through the UK Particle Physics and Astronomy Research Council (PPARC) grant number GR/L63952. We thank the World Data Centre at Rutherford Appleton Laboratory for use of computing facilities to carry out some of the simulations presented in this work.

References

Chapman, S., Lindzen, R.S., 1970. Atmospheric Tides. D. Reidel Publishing Co., Dordrecht.

Chiu, Y.T., 1975. An improved phenomenological model of ionospheric density. Journal of Atmospheric and Terrestrial Physics 37, 1563.

Fesen, C., 1997. Geomagnetic activity effects on thermospheric tides: a compendium of theoretical predictions. Journal of Atmospheric and Terrestrial Physics 59, 785–803.

Forbes, J.M., 1995. Tidal and Planetary Waves, Geophysical Monograph 87, American Geophysical Union.

Foster, J.C., Holt, J.M., Musgrove, R.G., Evans, D.S., 1986. Ionospheric convection associated with discrete levels of particle precipitation. Geophysical Research Letters 13, 656–659.

Fuller-Rowell, T.J., Rees, D., 1980. A three-dimensional time dependent global model of the thermosphere. Journal of Atmospheric Sciences 37, 2545–2567.

Fuller-Rowell, T.J., Rees, D., Quegan, S., Moffett, R.J., Bailey, G.J., 1987. Interactions between neutral thermospheric composition and the polar ionosphere using a coupled global model. Journal of Geophysical Research 92, 7744–7748.

Fuller-Rowell, T.J., Evans, D., 1987. Height-integrated Pederson and Hall conductivity patterns inferred from the TIROS-NOAA satellite data. Journal of Geophysical Research 92, 7606–7618.

Fuller-Rowell, T.J., Rees, D., Quegan, S., Moffett, R., Codrescu, M.V., Millward, G.H., 1996. A coupled thermosphere–ionosphere model (CTIM). In: Schunk, R.W. (Ed.) STEP Handbook of Ionospheric Models pp. 217–238.

Goncharenko, L.P., Salah, J.E., 1998. Climatology and variability of the semidiurnal tide in the lower thermosphere over Millstone Hill. Journal of Geophysical Research 103, 20,715–20,726.

Hagan, M.E., Forbes, J.M., Vial, F., 1995. On modelling migrating solar tides. Geophysical Research Letters 22, 893–896.

Hedin, A.E., 1991. Extension of the MSIS thermosphere model into the middle and lower atmosphere. Journal of Geophysical Research 96, 1159–1172.

Hedin, A.E., Fleming, E.L., Manson, A.H., Schmidlin, F.J., Avery, S.K., Clark, R.R., Franke, S.J., Fraser, G.J., Tsuda, T., Vial, F., Vincent, R.A., 1996. Empirical wind model for middle and lower atmosphere. Journal of Atmospheric and Terrestrial Physics 58, 1421–1447.

Holton, J.R., 1975. The dynamic meteorology of the stratosphere and mesosphere. Meteorological Monographs 15 (37), 53–75.

Johnson, R.M., Wickwar, V.B., Roble, R.G., Luhmann, J.G., 1987. Lower-thermospheric winds at high latitude: Chatanika radar observations. Annales de Geophysicae 5A, 383–404.

Kunitake, M., Schlegel, K., 1991. Neutral winds in the lower thermosphere at high latitudes from 5 years of EISCAT data. Annales Geophysicae 9, 143–155.

Larsen, M.F., Walterscheid, R.F., 1995. Modified geostrophy in the thermosphere. Journal of Geophysical Research 100, 17,321–17,330.

Lindzen, R.S., Blake, D., 1972. Lamb waves in the presence of realistic distributions of temperature and dissipation. Journal of Geophysical Research 77, 2166–2176.

Maeda, S., Fuller-Rowell, T.J., Evans, D.S., 1989. Zonally averaged dynamical and compositional response of the thermosphere to auroral activity during September 18–24, 1984. Journal of Geophysical Research 94, 16,869–16,883.

Maeda, S., Fujiwara, H., Nozawa, S., 1999. Momentum balance of dayside E region neutral winds during geomagnetically quiet summer days. Journal of Geophysical Research 104, 19,871–19,880.

Millward, G.H., Moffett, R.J., Quegan, S., Fuller-Rowell, T.J., 1996. A coupled thermosphere–ionosphere–plasmasphere model (CTIP). In: Schunk, R.W. (Ed.) STEP Handbook of Ionospheric Models pp. 239–279.

Nozawa, S., Brekke, A., 1995. Studies of the E region neutral wind in the disturbed auroral ionosphere. Journal of Geophysical Research 100, 14,717–14,734.

Quegan, S., Bailey, G.J., Moffett, R.J., Heelis, R.A., Fuller-Rowell, T.J., Rees, D., Spiro, A.W., 1982. A theoretical study of the distribution of ionization in the high-latitude ionosphere and the plasmasphere: first results on the mid-latitude trough and the light ion trough. Journal of Atmospheric and Terrestrial Physics 44, 619–640.

Richmond, A.D., Blanc, M., Emery, B.A., Wand, R.H., Fejer, B.G., Woodman, R.F., Ganguly, S., Amayenc, P., Behnke, R.A., Calderon, C., Evans, J.V., 1980. An empirical model of quiet-day

ionospheric electric fields at middle and lower latitudes. Journal of Geophysical Research 85, 4658–4664.

Rishbeth, H., Müller-Wodarg, I.C.F., 1999. Vertical circulation and thermospheric composition: a modelling study. Annales Geophysicae 17, 794–805.

Teitelbaum, H., Vial, F., 1991. On the tidal variability induced by non-linear interaction with planetary waves. Journal of Geophysical Research 96, 14,196–14,178.

Volland, H., 1988. Atmospheric tidal and planetary waves. Kluwer Academic Publishers, Dordrecht.

Wells, G.D., Rodger, A.S., Moffett, R.J., Bailey, G.J., Fuller-Rowell, T.J., 1997. The effects of nitric oxide cooling and the photodissociation of molecular oxygen on the thermosphere/ionosphere system over the Argentine Islands. Annales Geophysicae 17, 355–365.